Available online at www.sciencedirect.com
ScienceDirect
Advances in Water Resources 30 (2007) 984–997
Advances in Water Resources
www.elsevier.com/locate/advwatres

Concepts for measuring horizontal groundwater flow directions using the passive flux meter

Harald Klammler [a,b,c], Kirk Hatfield [a,b,*], Michael D. Annable [b,d]

[a] Department of Civil and Coastal Engineering, University of Florida, 365 Weil Hall, Gainesville, FL 32611-6450, United States
[b] Inter-Disciplinary Program in Hydrologic Sciences, University of Florida, Gainesville, FL 32611-6450, United States
[c] Department of Hydraulic Structures and Water Resources Management, Graz University of Technology, Austria
[d] Department of Environmental Engineering Sciences, Gainesville, FL 32611-6450, United States

Received 26 May 2006; received in revised form 26 July 2006; accepted 29 August 2006
Available online 31 October 2006

Abstract

The passive flux meter (PFM) is a permeable down-hole device designed to measure the *magnitudes* of horizontal groundwater specific discharge and contaminant mass flux in porous media. By means of a geometrical analysis of resident tracer transport inside a PFM, this paper introduces two new PFM designs capable of measuring both the direction and magnitude of horizontal water and contaminant fluxes. One design relies on the detection of a single resident tracer over multiple domains within the PFM cross section to determine the magnitude and direction of water flux. The second PFM configuration uses the detected loss of multiple resident tracers in different sectors of the PFM cross section to generate the same characterization of water flux. Both designs rely on the assumption of linear, instantaneous and reversible tracer sorption.
© 2006 Elsevier Ltd. All rights reserved.

Keywords: Contaminant; Aquifer; Hydrology

1. Introduction

Both the direction and magnitude of groundwater flow and contaminant mass flux are considered important parameters with respect to risk assessment and remediation of contaminated aquifers [4]. Over the last four decades, much of the literature has focused on quantifying the magnitudes of water and contaminant flows while little attention has been given to directional measures. The classic standard method of estimating the direction of flow uses a water table contour map, and a certain minimum number of observation wells in the area of interest. Natural gradient tracer tests have also been performed, but at the risk of not detecting tracers in observation wells situated too far apart (see for example [15,7]). Initially Drost et al. [6] and more recently Lamontagne et al. [12] describe a single borehole method (known as "point dilution test), which appears to ameliorate some of the problems associated with tracer studies. While the measurement of the magnitude of groundwater flux is based on the rate of dilution of a tracer in a borehole, for the measurement of the flow direction Drost et al. [6] propose the use of radioactive tracers that are washed out of the borehole in the direction of flow and are then detected by a respective probe installed in the borehole. A related method is described by White [18], in which a slug of salt water is injected in a well or pit. The movement of the slug is then traced using electric resistivity measurements by different electrode arrays on the surface. A more recent evaluation of borehole flow meters [17] compares measurements of three flow meters capable of making point estimates of the direction and magnitude of flow: (1) the heat-pulse flow meter described by Kerfoot [10,11] and Guthrie [8] as well as another

* Corresponding author. Address: Department of Civil and Coastal Engineering, University of Florida, 365 Weil Hall, Gainesville, FL 32611-6450, United States. Tel.: +1 352 3929536; fax: +1 352 3923394.
E-mail address: khatf@ce.ufl.edu (K. Hatfield).

0309-1708/$ - see front matter © 2006 Elsevier Ltd. All rights reserved.
doi:10.1016/j.advwatres.2006.08.007

related method using thermal perturbation [1], (2) the "acoustic doppler velocimeter" (ADV) developed by SonTek [13], and (3) the colloidal borescope developed by the US Department of Energy [16]. The latter two technologies have in common that they do not measure fluid movement directly but rather track the movement of naturally suspended particles in the water column of a borehole. The ADV relies on the acoustic Doppler effect to track the particle movement, while the colloidal borescope uses a video camera in combination with a black light source. The US Department of the Interior [17] determined that both methods require further study to provide reliable directional measurement; hence, the development of an alternative, in particular a passive method, is of interest. Still another method based on thermal perturbation is the in situ permeable flow sensor [3], which is directly installed in the ground (no disturbance by monitoring well, but instrument cannot be recovered after measurement) and which is capable of measuring the full three-dimensional groundwater flow velocity vector in unconsolidated, saturated, and porous media.

Hatfield et al. [9] and Annable et al. [2] developed and field-tested a new method to simultaneously measure the magnitudes of groundwater and contaminant fluxes in the porous subsurface. The method uses a permeable, sorptive device referred to as the passive flux meter (PFM) in the shape of a homogeneous, vertically segmented cylinder. This device is installed in a well or borehole for a specified period of time where it passively intercepts groundwater and contaminant flow. The PFM initially contains a known amount of one (or more) resident tracer(s) that is eluted from the PFM during the time of exposure to groundwater flow. The relative residual mass of resident tracer left on a particular vertical segment of the PFM after removal from the borehole is used to determine the cumulative groundwater flux over the time of exposure. Simultaneously to the elution of the resident tracer, the sorptive matrix of the PFM retains contaminants from the groundwater. The mass of each contaminant retained on the PFM is then used to determine the cumulative contaminant mass flux over the time of exposure.

The purpose of the present work is to develop the concepts and compare the usefulness of two different PFM configurations that allow for the simultaneous measurement of both the direction and magnitude of groundwater and contaminant flux. The new configurations specifically enable measurements of groundwater flow direction, and it is assumed this direction is the same for contaminant flow. Measurements of the magnitudes of groundwater and contaminant mass fluxes remain as described in the original PFM configuration [9,2]. The cross section of the PFM of the first configuration (hereafter referred to as "ring" configuration) is depicted in Fig. 1 and was originally proposed and tested by Campbell et al. [5] to measure magnitude and direction of groundwater and contaminant flux at a bench scale in the laboratory. In this configuration, the cross section of the PFM is divided into four

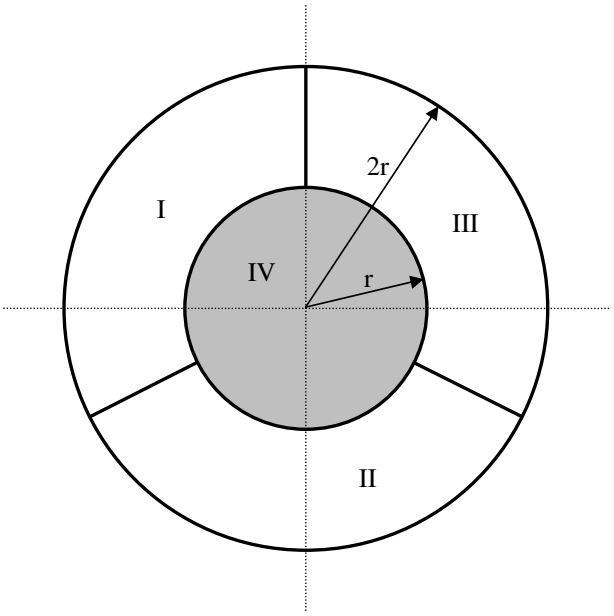

Fig. 1. Cross section of PFM – ring configuration.

sub areas where only the shaded center circle (area "IV") contains the resident tracer. Groundwater migrating through the PFM displaces the resident tracer into the surrounding ring that still consists of the same permeable, sorptive material as the center circle, but does initially not contain any resident tracer. Separate analyses of the four sub areas after removal from the borehole reveal the respective amounts of resident tracer in each of them, which are subsequently used to obtain an estimate of the direction of groundwater and contaminant flow.

The second configuration (hereafter referred to as "sector" configuration) is illustrated in Fig. 2 and represents an

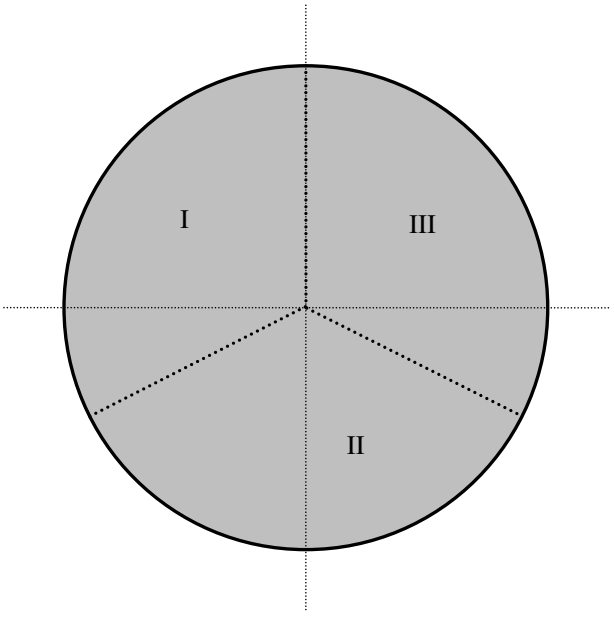

Fig. 2. Cross section of PFM – sector configuration.

alternative to the ring configuration of Fig. 1. Here, the cross sectional area of the PFM is divided into three equal sectors, where each contains one or more different resident tracers. Groundwater displaces the resident tracers in the direction of the flow, thus partially eluting them from the PFM. From the analysis of the whole cross sectional area, the remaining amounts of each resident tracer are determined and subsequently used to estimate the direction and magnitude of groundwater flow.

In order to evaluate and compare the two configurations, some practical aspects are discussed, and the theoretically exact calibration curves (curves relating the resulting amounts of resident tracers from the measurement to the required direction of flow) for both configurations are derived. The underlying assumptions for both configurations are that the direction of flow does not vary during the time of exposure, and that the vertical flow component in the PFM can be neglected with respect to the horizontal one. For the derivation of the calibration curves it is furthermore assumed that tracer sorption is linear, instantaneous (equilibrium) and reversible as well as independent of other resident tracers. Diffusive and dispersive transport is neglected with respect to convective transport. Campbell et al. [5] use an approximate calibration method for the ring configuration, which in turn does not require some of these assumptions, and which is discussed with respect to the results presented.

2. The ring configuration

Under the above stated assumptions, exposure to groundwater flow for a certain time displaces every tracer (for brevity, "resident" is omitted hereafter) molecule by the same displacement vector of length q_r [L] and direction q_θ [°]. This results in a mere parallel displacement of the entire circularly shaped tracer plume, thus preserving the initial shape as shown in Fig. 3. Hatfield et al. [9] use this fact to adopt a rectilinear stream tube tracer transport model inside the PFM to derive the relationship between the volume of water conveyed through the PFM and the mass of tracer eluted from (or remaining in) the PFM. Although Hatfield et al. [9] also present methods to account for non-linear and non-equilibrium tracer sorption in this relationship, the present derivation only makes use of the solution for linear and equilibrium sorption. The inclusion of non-linear and/or non-equilibrium sorption for the measurement of flow direction is not straightforward due to the more complex configuration of the PFM and possible effects will be discussed below. The relative distance q_r/r [–], with r [L] being the radius of the tracer plume, is thus obtained from Hatfield et al. [9] as

$$\frac{q_r}{r} = \frac{1 - m_{IV}}{0.6} \tag{1}$$

where m_{IV} [–] is the relative amount of tracer remaining in the center area IV after exposure to groundwater flow with respect to the total amount of tracer initially present in area IV. Eq. (1) is an approximate relationship being accurate for $q_r/r < 1.2$ and q_r/r represents twice the "dimensionless cumulative pore volume of fluid intercepted by the device" as defined by Hatfield et al. [9].

Knowing q_r/r and the relative amounts of tracer m_I [–], m_{II} [–] and m_{III} [–] displaced into areas I, II and III respectively, it is possible to infer the direction q_θ of the displacement. In a geometrical interpretation, m_I, m_{II}, m_{III} and m_{IV} represent the portions of the shaded circle intersecting with areas I, II, III, and IV, respectively. Since each combination of q_r/r (for $0 \leqslant q_r/r \leqslant 1$) and q_θ results in a unique combination of values for m_I, m_{II}, and m_{III} (m_{IV} only depends on q_r/r), q_θ can be determined from the other variables. In the sequel, the functions $m_I(q_r/r, q_\theta)$, $m_{II}(q_r/r, q_\theta)$, and $m_{III}(q_r/r, q_\theta)$ are derived and graphically represented in order to invert them to obtain q_θ. Thanks to the equally shaped sectors that are only shifted by an angle of $\pm 120°$ with respect to each other, it is sufficient to find one of the three functions. The other two functions are then simply obtained by a linear transformation using $(q_\theta \pm 120°)$ instead of q_θ. This coordinate transformation and taking advantage of symmetry of the sub areas of the ring reduce the problem to finding, for example, $m_I(q_r/r, q_\theta)$ for $-30° \leqslant q_\theta \leqslant 150°$, which corresponds to the half plane on the upper side of the axis of symmetry of area I as indicated in Fig. 3. Since for $q_r/r > 1$, q_θ can no longer be unambiguously determined from m_I, m_{II}, and m_{III} in all cases (tracer might only be detected in a single ring sector, thus leaving a range of possible flow directions), the following derivation is restricted to a range of $0 \leqslant q_r/r \leqslant 1$. Under these conditions three different cases have to be distinguished in order to be able to express m_I as a function of the displacement vector (q_r, q_θ). In the following derivations, r will be kept as a parameter to facilitate a better understanding. Fig. 3 gives an example of the shape of the area representing m_I

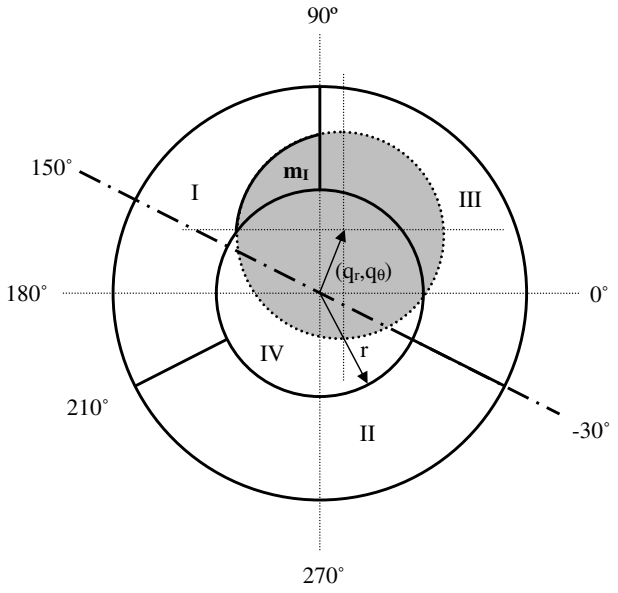

Fig. 3. Displacement of tracer plume by a vector (q_r, q_θ) – case one.

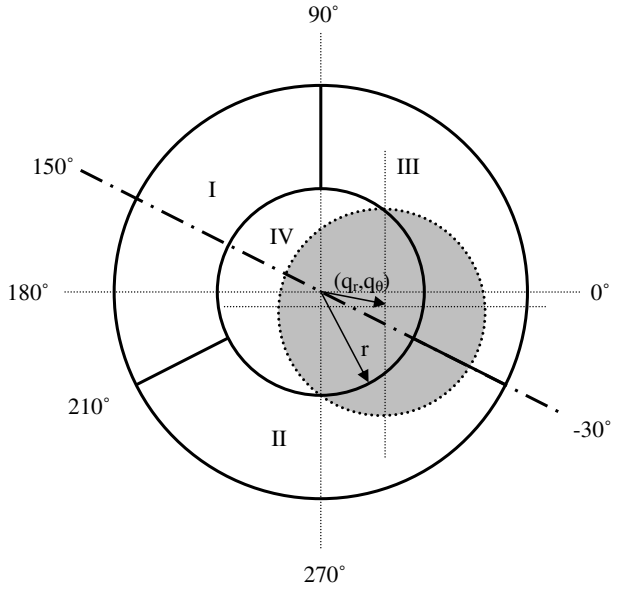

Fig. 4. Displacement of tracer plume by a vector (q_r, q_θ) – case two.

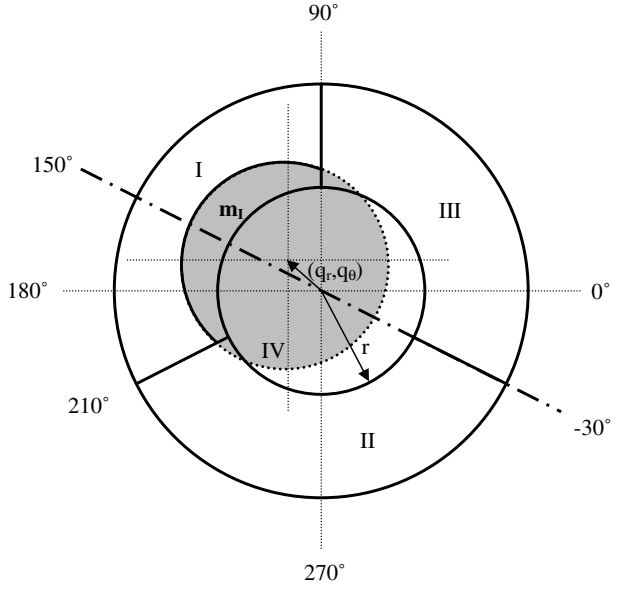

Fig. 5. Displacement of tracer plume by a vector (q_r, q_θ) – case three.

for case one, and Figs. 4 and 5 give respective examples for the two remaining cases.

In case one, two circumferences and one straight line border m_I, while m_I is zero in case two and bordered by two circumferences and two straight lines in case three. Since case one may be regarded as the transition case between cases two and three, the only transition conditions that have to be found are those between cases one and two and between one and three. Fig. 6 illustrates the situation when cases one and two pass over into each other. The base angle δ of the isosceles triangle with the sides q_r, r and r takes the value $(90° - q_\theta)$, and knowing $\cos\delta = q_r/2r$, one obtains the transition condition for q_r/r as a function of q_θ as follows:

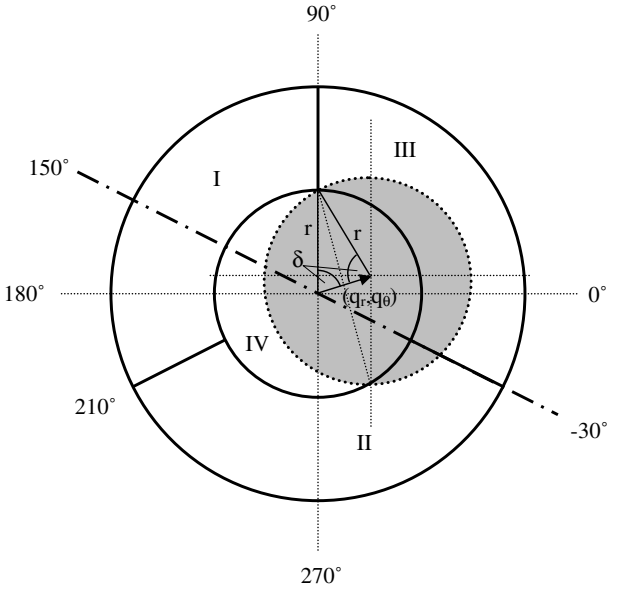

Fig. 6. Transition between cases one and two.

$$\frac{q_r}{r} = 2 \cdot \cos(90° - q_\theta) = 2 \cdot \sin q_\theta \tag{2}$$

Fig. 6 also shows that for actual values of q_r/r higher than the respective value obtained from Eq. (2), case two prevails, while otherwise it is case one. Fig. 7 illustrates the second transition between cases one and three. Here the base angle δ of the isosceles triangle takes the value $(210° - q_\theta)$ and one obtains the following transition condition for q_r/r as a function of q_θ:

$$\frac{q_r}{r} = 2 \cdot \cos(210° - q_\theta) \tag{3}$$

Again, it may be seen from inspection of Fig. 7 that case one prevails if the actual q_r/r is higher than the q_r/r of Eq. (3) and if it is lower, it is case three. Fig. 8 shows the

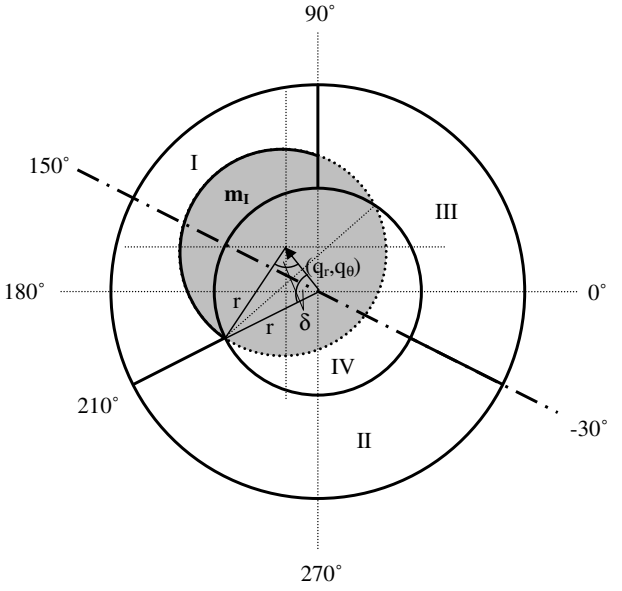

Fig. 7. Transition between cases one and three.

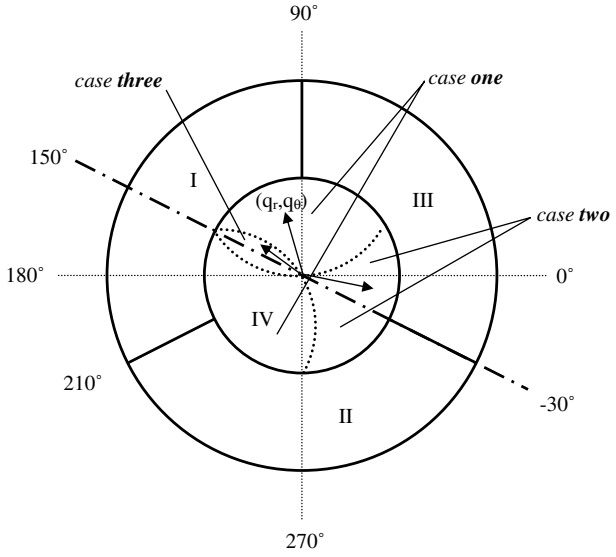

Fig. 8. Cross section of PFM with borders between the three cases.

cross section of the device with the borders (dotted lines) between the three cases according to Eqs. (2) and (3). It can be alternatively used to determine what case is obtained dependent on where the displacement vector (q_r, q_θ) points.

In order to calculate the area $m_{I,one}$ (case one) equivalent to the curvilinear triangle (HJK) in Fig. 9, which represents the amount of tracer displaced into sub area I, the areas A_1 (FJG) and A_2 (GHK) are subtracted from the sector (FJK). (Note that Figs. 9–11 for a better illustration now only display the center region of the PFM cross section.) Knowing that the area of a sector of a circle can be expressed as half of the radius times the circumference (which equals the radius times the center angle in radians), m_I can be written in a dimensionless form with respect to the total area where the tracer is present as

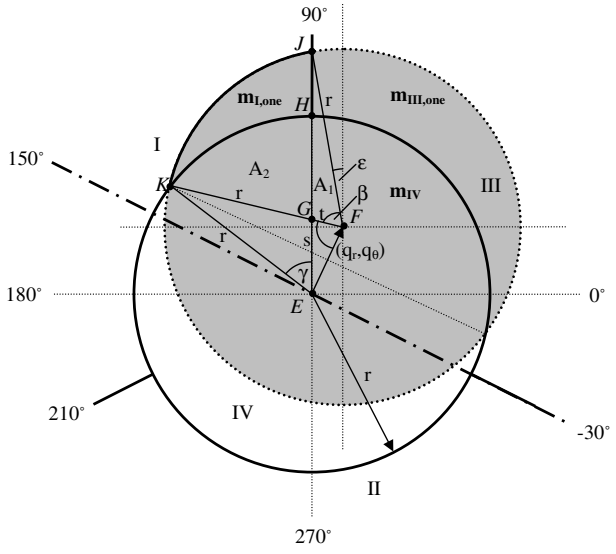

Fig. 9. Calculation of area $m_{I,one}$ (case one) for $0° \leqslant q_\theta \leqslant 90°$ (only center region shown).

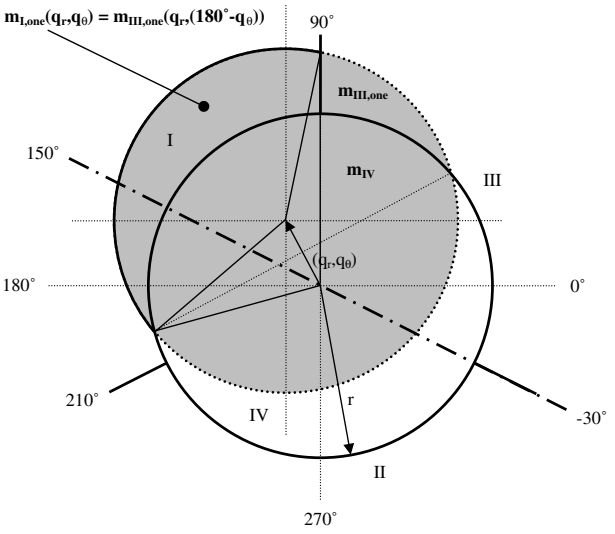

Fig. 10. Calculation of area $m_{I,one}$ (case one) for $90° \leqslant q_\theta \leqslant 150°$ (only center region shown).

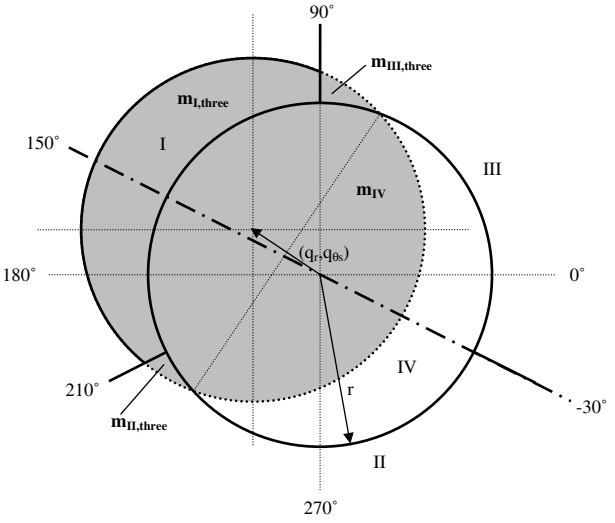

Fig. 11. Calculation of area $m_{I,three}$ (case three; only center region shown).

$$m_{I,one}(q_r, q_\theta) = \frac{1}{r^2\pi} \cdot \left(\frac{r^2 \cdot \beta_{rad}}{2} - A_1 - A_2 \right) \tag{4}$$

The index "rad" indicates that the respective angle has to be used in radians. Using the fact that the area of a triangle can be obtained as half of the product of two sides times the sine of the angle that the two sides enclose, A_1 and A_2 become

$$A_1 = \frac{r \cdot t}{2} \cdot \sin\beta \tag{5}$$

$$A_2 = \frac{r^2 \cdot \gamma_{rad}}{2} - \frac{r \cdot s}{2} \cdot \sin\gamma \tag{6}$$

The auxiliary variables s (distance (EG)), t (distance (FG)), β (angle (GFJ)) and γ (angle (KEG)) are expressed with the help of δ (angles (KEF) and (KFE)) and ε (angle (JF) to vertical) as performed in Eqs. (7)–(12). The operations in-

volved hereby are the standard ones for right-angled triangles as well as the sine law for general triangles, which implies that the ratios of each side and their respective sines of the opposite angles are equal

$$\frac{s}{\sin\delta} = \frac{q_r}{\sin[\pi - \delta - (\delta - \gamma)]} \Rightarrow s = q_r \cdot \frac{\sin\delta}{\sin(2\delta - \gamma)} \tag{7}$$

$$\frac{t}{\sin(\delta - \gamma)} = \frac{q_r}{\sin[\pi - \delta - (\delta - \gamma)]} \Rightarrow t = q_r \cdot \frac{\sin(\delta - \gamma)}{\sin(2\delta - \gamma)} \tag{8}$$

$$\beta = 90^\circ - \underbrace{[(90^\circ - q_\theta) - (90^\circ - \delta)]}_{\text{angle}(FK)\text{to horizontal}} - \varepsilon = 90^\circ + q_\theta - \delta - \varepsilon \tag{9}$$

$$\gamma = q_\theta + \delta - 90^\circ \tag{10}$$

$$\delta = \arccos\frac{q_r}{2r} \tag{11}$$

$$\varepsilon = \arcsin\left(\frac{q_r}{r} \cdot \cos q_\theta\right) \tag{12}$$

Substituting these six equations in Eqs. (5) and (6), and subsequent substitution of Eqs. (5) and (6) in Eq. (4) result in an expression for $m_{I,one}$ as a function of q_r and q_θ only. However, inspection of Fig. 10 shows that Eqs. (4)–(12) are no longer valid as soon as q_θ exceeds 90°. Yet, it may be recognized that $m_{III,one}$ for $0^\circ \leqslant q_\theta \leqslant 90^\circ$ of Fig. 9 and $m_{I,one}$ for $90^\circ \leqslant q_\theta \leqslant 150^\circ$ of Fig. 10 are symmetric about the vertical axis, thus possessing the same area. Mathematically, the condition for this symmetry are equal q_r in both cases and that q_θ in Fig. 9 is equal to $(180^\circ - q_\theta)$ in Fig. 10. In other words, if these conditions are met, $m_{I,one}$ of Fig. 10 is equal to $m_{III,one}$ of Fig. 9, which can be calculated as

$$\begin{aligned} m_{I,one}(q_r, q_\theta) &= m_{III,one}(q_r, (180^\circ - q_\theta)) \\ &= 1 - m_{I,one}(q_r, (180^\circ - q_\theta)) - m_{IV}(q_r) \\ &\quad \text{for } 90^\circ \leqslant q_\theta \leqslant 150^\circ \end{aligned} \tag{13}$$

since $m_{II,one}$ is always zero. $m_{I,one}(q_r,(180^\circ - q_\theta))$ in Eq. (13) is evaluated from Eq. (4) while m_{IV} from Eq. (13) is already previously required for computing q_r and is derived by Hatfield et al. [9] as reproduced in Eq. (14)

$$m_{IV}(q_r) = \frac{2}{\pi} \cdot \left[\arcsin\sqrt{1 - \left(\frac{q_r}{2r}\right)^2} - \frac{q_r}{2r} \cdot \sqrt{1 - \left(\frac{q_r}{2r}\right)^2}\right] \tag{14}$$

Note: Eq. (1), which is used in practice for the determination of q_r/r, is nothing but the linearized, approximate inverse function of Eq. (14).

In summary, within the boundaries of case one as defined in Fig. 8, Eq. (4) is used to evaluate m_I for $0^\circ \leqslant q_\theta \leqslant 90^\circ$ and Eq. (13) for $90^\circ \leqslant q_\theta \leqslant 150^\circ$.

From Fig. 4 it is easily seen that m_I for case two is always zero

$$m_{I,two} = 0 \tag{15}$$

Finally, for case three, m_I is obtained from a combination of the above derived equations as inspection of Fig. 11 demonstrates

$$m_{I,three}(q_r, q_\theta) = 1 - m_{II,three}(q_r, q_\theta) - m_{III,three}(q_r, q_\theta) - m_{IV}(q_r) \tag{16}$$

m_{IV} is again known from Eq. (14), and $m_{II,three}$ and $m_{III,three}$ are obtained by taking advantage of the solution for case one from Eq. (4) (the second solution of Eq. (13) is not relevant here)

$$m_{II,three}(q_r, q_\theta) = m_{I,one}(q_r, (q_\theta - 120^\circ)) \tag{17}$$

$$m_{III,three}(q_r, q_\theta) = m_{I,one}(q_r, (180^\circ - q_\theta)) \tag{18}$$

Substituting Eqs. (17) and (18) in Eq. (16) results in m_I for case three as a function of q_r and q_θ. Knowing the analytical solutions for m_I for the three possible cases and knowing the transition conditions from one case to another, m_I may now be plotted as a function of q_r and q_θ in a range of $0 \leqslant q_r \leqslant 1$ and $-30^\circ \leqslant q_\theta \leqslant 150^\circ$. The results for the remaining range of q_θ from 150° to 330° are obtained by using symmetry. Figs. 12 and 13 demonstrate how the amount of tracer displaced into sub area I changes with direction q_θ when the cumulative flux q_r is kept constant and vice verse. In order to determine the same kind of curves for sub areas II and III, the curves for sub area I are simply shifted by 120° to the right and to the left, respectively. Fig. 14 finally shows an example of how q_θ can be determined from the measured quantities m_I, m_{II} and m_{III} for an arbitrarily chosen q_r/r of 0.9. Due to symmetry, for one sub area two possible values of q_θ are obtained. The result of a second sub area then confirms one of the two solutions, which is then interpreted as the mea-

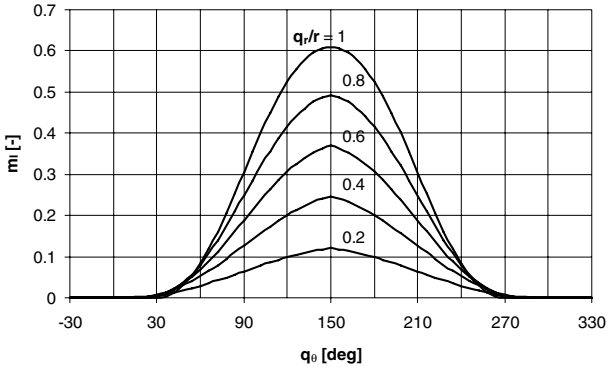

Fig. 12. m_I as a function of q_θ for certain q_r/r's.

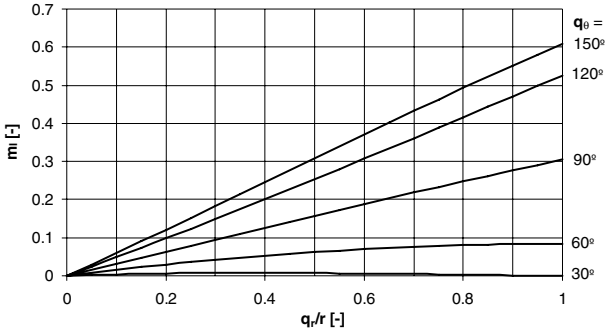

Fig. 13. m_I as a function of q_r/r for certain q_θ's.

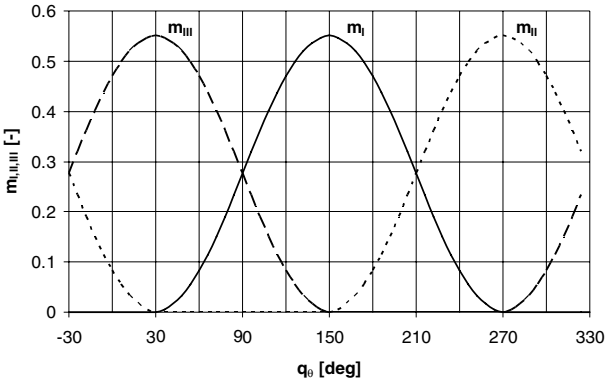

Fig. 14. m_{I}, m_{II} and m_{III} for $q_{\mathrm{r}}/r = 0.9$.

sured direction of flow. The third sub area never contains practically any tracer ($m \approx 0$) and consequently does not contribute any significant information to the determination of q_θ.

The above solution is geometrically exact and relies on the assumption that the initial circular shape of the tracer plume is preserved. Campbell et al. [5] apply an approximate method to interpret the measurements of their experiments. They assume that the amounts of tracer detected in the sub areas I–III are concentrated in the centers of mass of the respective sub areas and subsequently calculate the location of the overall center of mass from the three point masses. The argument of the polar coordinates of the overall center of mass is regarded as the estimate for the direction of flow and can be shown to be

$$q_\theta = \arctan\frac{(m_{\mathrm{III}} + m_{\mathrm{I}}) \cdot \sin 30^\circ - m_{\mathrm{II}}}{(m_{\mathrm{III}} - m_{\mathrm{I}}) \cdot \cos 30^\circ} \tag{19}$$

for a PFM orientation as used above. Eq. (19) is valid for displacements with a horizontal component to the right. If the horizontal component is seen to be directed to the left (from inspection of the cartesian coordinates of the overall center of mass), then q_θ from Eq. (19) has to be corrected by $\pm 180^\circ$.

Knowing the exact functions for m_{I}, m_{II} and m_{III} of q_{r} and q_θ from above, the systematic error implicit in the center of mass approximation can be quantified. The result is shown in Fig. 15 where the deviations of the two curves for $q_{\mathrm{r}}/r = 0.1$ (thin) and $q_{\mathrm{r}}/r = 1$ (thick) from the straight line represent the systematic error in the estimation. The errors are seen to vanish for directions parallel to each axis of symmetry of the cross section of the PFM. For directions in between those axes of symmetry the maximum error is comprised in an interval of approximately $\pm 20^\circ$, which lies within the expected range of accuracy of the measurement. The center of mass method does not require that the circular shape of the tracer plume is preserved and its application is independent of the q_{r} estimate. This fact is of particular interest in cases where the sorption behavior is no longer linear, resulting in a longitudinal stretching (“tailing”) of the initially circular tracer plume as it was the case in the experiments reported by Campbell et al. [5].

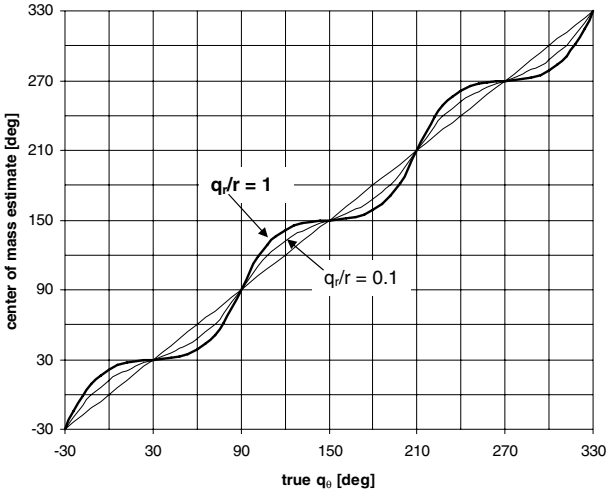

Fig. 15. Systematic error of center of mass approximation.

3. The sector configuration

This configuration as introduced in connection with Fig. 2 divides the cross sectional area of the PFM into three equal sectors where each of them contains a different tracer in addition to the tracer that is present over the whole circle and that is used for the determination of q_{r}. Adopting the same assumptions about tracer transport as discussed with the ring configuration, the tracers are again displaced by a distance q_{r} in the direction q_θ of water flow, thus preserving the initial shapes (sectors of a circle) of their plumes. Dependent on the displacement vector with respect to the orientation of the PFM, more or less of each tracer is eluted from the PFM, and measurement of the remaining tracer masses can be used to determine the direction of flow. The magnitude q_{r} of the displacement vector depends on the retardation of a particular tracer and, thus, may vary between tracers. However, since the tracers are considered as completely independent as to their sorption properties, each of them can be investigated separately. The value q_{r} for a given tracer in a sector is calculated from taking the product of the known q_{r} of the tracer initially present over the whole cross section and the ratio obtained from dividing the retardation factor of this tracer by the retardation factor of the tracer in the respective sector.

In analogy to the ring configuration, the amounts (areas) of the three tracers in the sectors remaining in the PFM after exposure to groundwater flow have to be determined as a function of their displacement vectors in order to evaluate q_θ from the measured data. Again, rotational symmetry reduces the problem to deriving this function for one single tracer (such as tracer I), and symmetry with respect to the direction $-30^\circ/150^\circ$ for that tracer is used to restrict the required observation to one half plane. Knowing this, the relationship is established between the amount m_{I} of tracer I remaining in the PFM relative to its initial amount (one sector) and the displacement vector for a range of $0 \leqslant q_{\mathrm{r}}/r \leqslant 1$ and $-30^\circ \leqslant q_\theta \leqslant 150^\circ$. $q_{\mathrm{r}}/r > 1$ is not considered here for analogous reasons as given with

the ring configuration. Cases may occur where only one tracer is left in the PFM, thus permitting a range of different possible flow directions leading to ambiguous measurements.

Under the conditions stated, three different cases have to be distinguished in order to be able to express $m_I(q_r, q_\theta)$ analytically. Figs. 16–18 give an example for each case, assuming, without loss of generality, that the tracers are equally retarded. In case one, the two straight sides of the sector and both circumferences border the remaining area of tracer I, while in case two and three only one circumference is involved. Since case one actually may be regarded as the transition case between cases two and three, the only transition conditions to be found are those

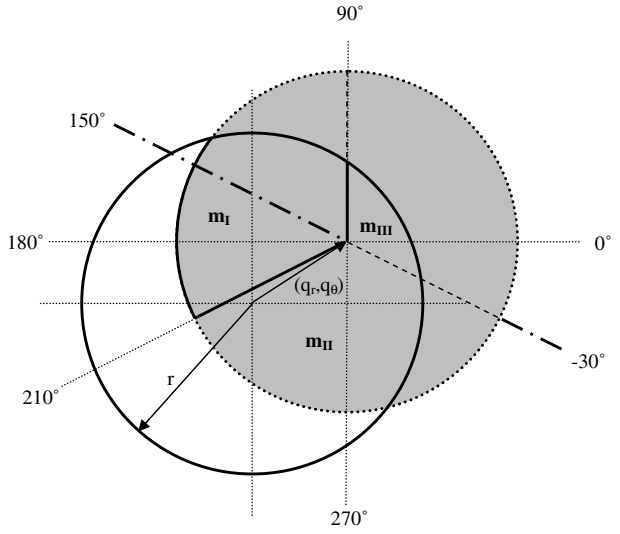

Fig. 16. Displacement of tracer plume by a vector (q_r, q_θ) – case one.

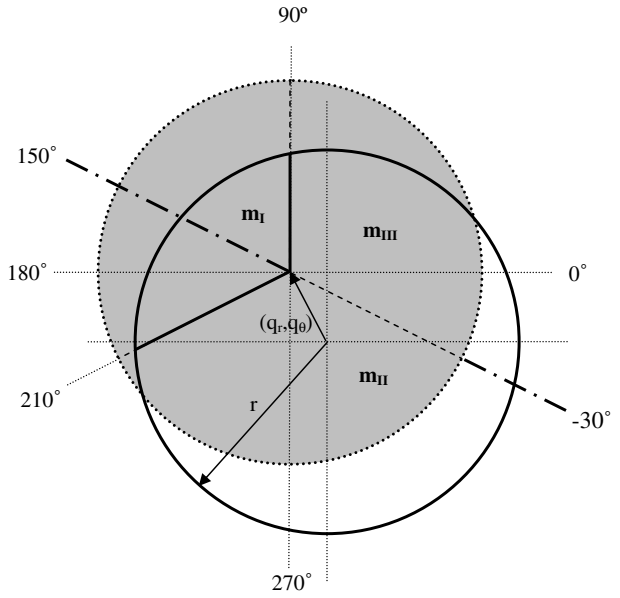

Fig. 17. Displacement of tracer plume by a vector (q_r, q_θ) – case two.

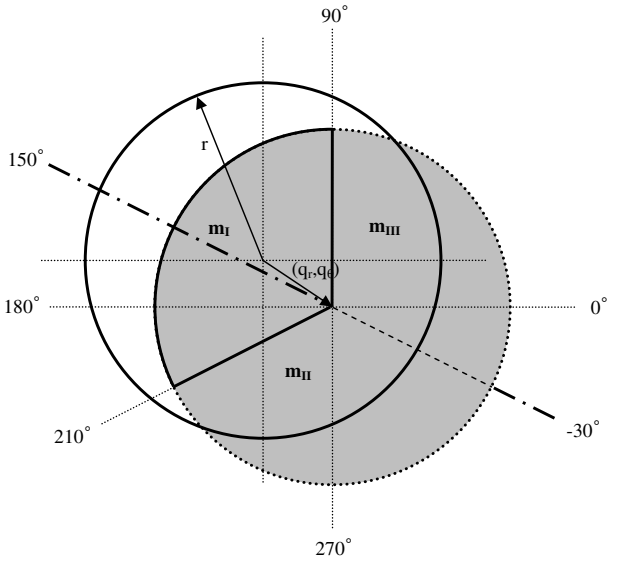

Fig. 18. Displacement of tracer plume by a vector (q_r, q_θ) – case three.

between cases one and two and between cases one and three. Following the same steps as performed for the ring configuration one obtains for the transition between cases one and two as shown in Fig. 19

$$\frac{q_r}{r} = 2 \cdot \cos\delta = 2 \cdot \cos(q_\theta - 30^\circ) \tag{20}$$

Case two prevails for actual q_r/r's higher than the one given by Eq. (20) and case one if it is lower. From Fig. 20 the transition condition between cases one and three can be seen to be

$$\frac{q_r}{r} = 2 \cdot \cos\delta = 2 \cdot \cos(q_\theta - 90^\circ) \tag{21}$$

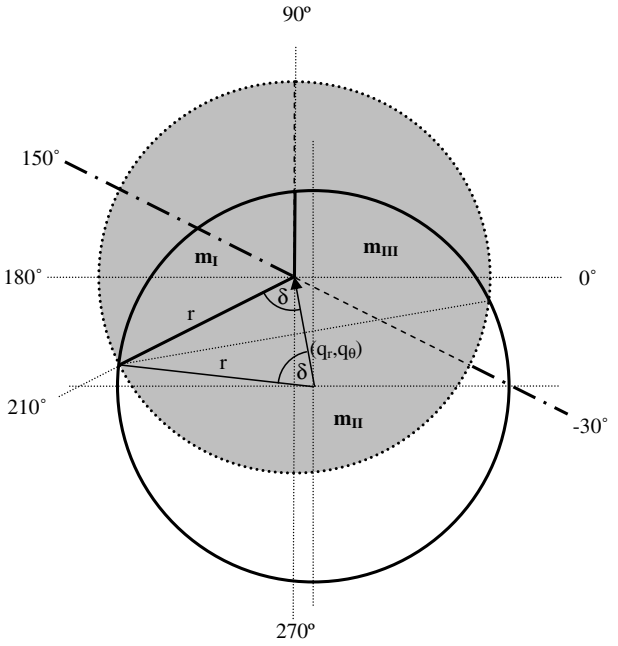

Fig. 19. Transition between cases one and two.

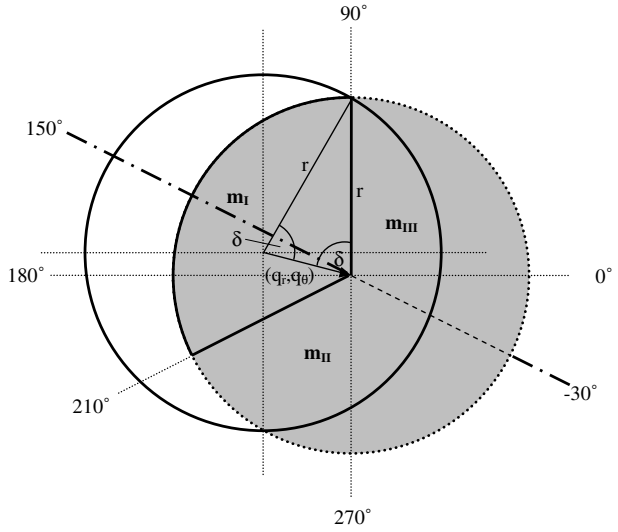

Fig. 20. Transition between cases one and three.

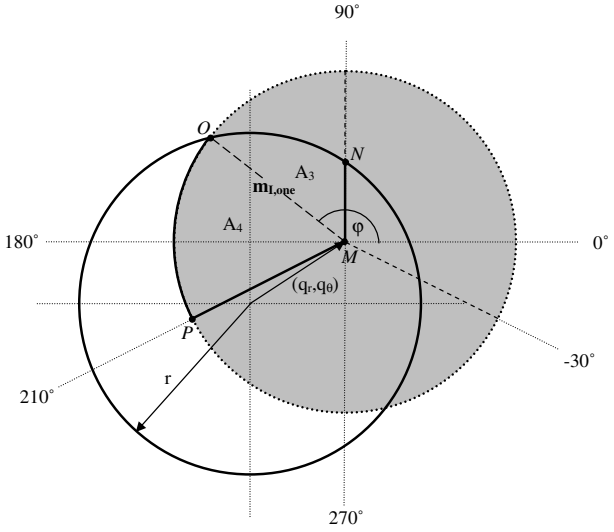

Fig. 22. Calculation of $m_{\mathrm{I,one}}$ (tracer I for case one).

where case one is obtained if q_r/r of Eq. (21) is exceeded and case three otherwise. The results of Eqs. (20) and (21) are illustrated in Fig. 21.

Finding the expression for $m_{\mathrm{I,one}}$ (q_r, q_θ), the relative amount of tracer I remaining in the PFM as a function of the displacement vector, requires dividing the area $(MNOP)$ representing $m_{\mathrm{I,one}}$ into area A_3 (MNO) and the sector A_4 (MOP) as illustrated in Fig. 22. A_3 is calculated with the help of Fig. 23 by subtraction of the areas A_5 (MSN) and A_6 (MOT) from the area of the half circle. A_5 is equal to the difference of the areas of the sector (QSN) and the triangle (QMN), as it is expressed in

$$A_5 = \frac{r^2 \cdot \beta_{1,\mathrm{rad}}}{2} - \frac{q_r \cdot r}{2} \cdot \sin\beta_1 = \frac{r^2}{2} \cdot \left(\beta_{1,\mathrm{rad}} - \frac{q_r}{r} \cdot \sin\beta_1\right) \quad (22)$$

β_1 is obtained from the other two angles of the triangle (QMN)

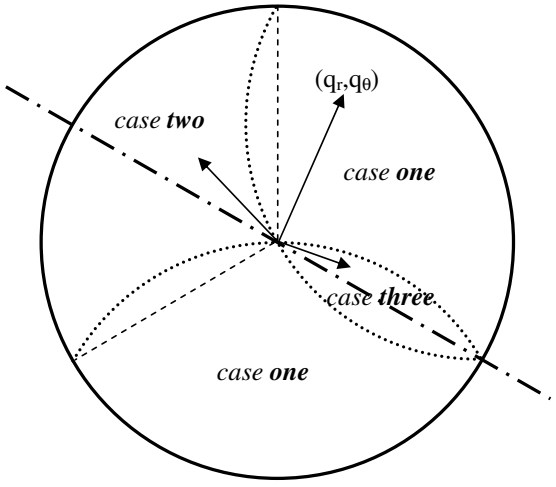

Fig. 21. Cross section of PFM with borders between the three cases.

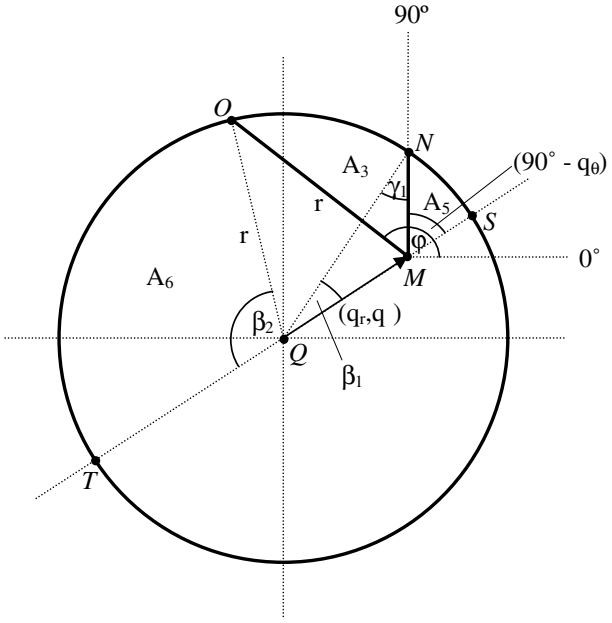

Fig. 23. Calculation of A_3.

$$\beta_1 = 180^\circ - \gamma_1 - [180^\circ - (90^\circ - q_\theta)] = 90^\circ - q_\theta - \gamma_1 \quad (23)$$

γ_1 is determined by using the sine law for triangles as Eq. (24) shows

$$\frac{\sin\gamma_1}{q_r} = \frac{\sin[180^\circ - (90^\circ - q_\theta)]}{r} \quad (24)$$

Using the standard relationship $\sin(90^\circ \pm x) = \cos x$, γ_1 results in

$$\gamma_1 = \arcsin\left[\frac{q_r}{r} \cdot \cos q_\theta\right] \quad (25)$$

Substitution of Eqs. (25) and (23) in Eq. (22) results in an expression for A_5 as a function of q_r and q_θ.

Also according to Fig. 23, area A_6 can be expressed as the total of the sector (QOT) of the circle and the triangle (QMO) as

$$A_6 = \frac{r^2 \cdot \beta_{2,\mathrm{rad}}}{2} + \frac{q_\mathrm{r} \cdot r}{2} \cdot \sin(180^\circ - \beta_2)$$
$$= \frac{r^2}{2} \cdot \left(\beta_{2,\mathrm{rad}} + \frac{q_\mathrm{r}}{r} \cdot \sin\beta_2\right) \quad (26)$$

where β_2 is obtained using the fact that the triangle (QMO) is isosceles (being the distances (QO) and (MO) equal to the radius r)

$$\beta_2 = 180^\circ - \arccos\frac{q_\mathrm{r}}{2r} \quad (27)$$

Substitution of Eq. (27) in Eq. (26) results in an expression for A_6 as a function of q_r alone.

The area A_4 of Fig. 22 is equal to the sector (MOP). Knowing from Fig. 22 that the angle (PMO) of this sector is $(210^\circ - \phi)$, and from Fig. 23 that $\varphi = \beta_2 + q_\theta$, A_4 can be written as

$$A_4 = \frac{r^2}{2} \cdot (210^\circ - \varphi)_\mathrm{rad} = \frac{r^2}{2} \cdot (210^\circ - q_\theta - \beta_2)_\mathrm{rad} \quad (28)$$

Eqs. (22), (26) and (28) are now combined according to

$$m_{\mathrm{I,one}}(q_\mathrm{r}, q_\theta) = \frac{A_3 + A_4}{\frac{r^2\pi}{3}} = \frac{3}{r^2\pi} \cdot \left(\frac{r^2\pi}{2} - A_5 - A_6 + A_4\right) \quad (29)$$

and since β_1 and β_2 are known as functions of q_r and q_θ, $m_{\mathrm{I,one}}$ is obtained as a function of q_r and q_θ as expressed in

$$m_{\mathrm{I,one}}(q_\mathrm{r}, q_\theta) = \frac{3}{2\pi} \cdot \left[\frac{13\pi}{6} - q_{\theta,\mathrm{rad}} - \beta_{1,\mathrm{rad}} - 2\beta_{2,\mathrm{rad}} + \frac{q_\mathrm{r}}{r}(\sin\beta_1 - \sin\beta_2)\right] \quad (30)$$

This expresses the relative remaining amount of tracer I for case one of Fig. 21.

The relative remaining amount of tracer I for case two $m_{\mathrm{I,two}}$ (see Fig. 17) can be calculated according to Fig. 24 as the area of a sector of the circle minus the areas A_7 and A_8 of the two triangles

$$m_{\mathrm{I,two}}(q_\mathrm{r}, q_\theta) = \frac{3}{r^2\pi} \cdot \left(\frac{r^2}{2} \cdot (\beta_{3,\mathrm{rad}} + \beta_{4,\mathrm{rad}}) - \frac{q_\mathrm{r} \cdot r}{2} \cdot \sin\beta_3 - \frac{q_\mathrm{r} \cdot r}{2} \cdot \sin\beta_4\right)$$
$$m_{\mathrm{I,two}}(q_\mathrm{r}, q_\theta) = \frac{3}{2\pi} \cdot \left[\beta_{3,\mathrm{rad}} + \beta_{4,\mathrm{rad}} - \frac{q_\mathrm{r}}{r} \cdot (\sin\beta_3 + \sin\beta_4)\right] \quad (31)$$

Performing the same operations as for the determination of β_1 in Eq. (23), β_3 and β_4 may be expressed as

$$\beta_3 = q_\Theta - \gamma_3 - 90^\circ \quad (32)$$
$$\beta_4 = 210^\circ - q_\Theta - \gamma_4 \quad (33)$$

and γ_3 and γ_4 are determined in the same way as γ_1 in Eq. (25)

$$\gamma_3 = \arcsin\left[\frac{q_\mathrm{r}}{r} \cdot \sin(q_\theta - 90^\circ)\right] = -\gamma_1 \quad (34)$$
$$\gamma_4 = \arcsin\left[\frac{q_\mathrm{r}}{r} \cdot \sin(210^\circ - q_\theta)\right] = \arcsin\left[\frac{q_\mathrm{r}}{r} \cdot \sin(q_\theta - 30^\circ)\right] \quad (35)$$

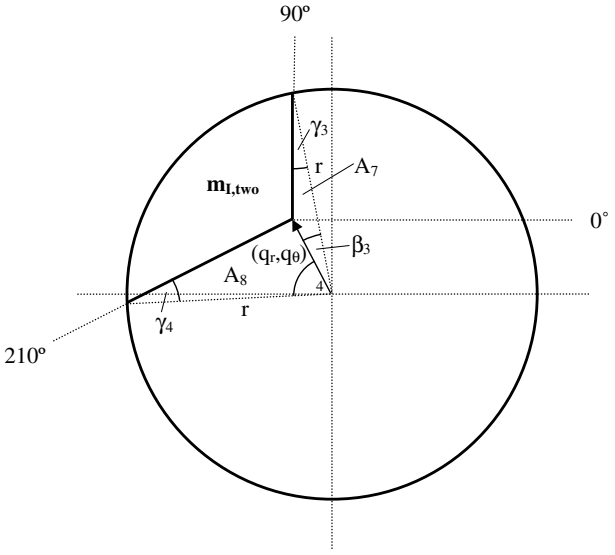

Fig. 24. Calculation of $m_{\mathrm{I,two}}$ (tracer I for case two).

Substitution of the last four equations into Eq. (31) results in an expression for $m_{\mathrm{I,two}}$ as a function of q_r and q_θ, which is valid for case two of Fig. 21.

As Fig. 18 demonstrates, none of tracer I is eluted from the PFM for case three, resulting in

$$m_{\mathrm{I,three}} = 1 \quad (36)$$

In analogy to the ring configuration, the analytical expressions for m_I derived above for the three possible cases are combined according to their transition conditions and graphically represented in Figs. 25–27, which directly correspond to Figs. 12–14 for the ring configuration. For the practical use in the laboratory or in the field where the m's and q_r's are known for every tracer, two values of q_θ are obtained from Fig. 27 for one tracer. This means that the result of a second tracer would already be sufficient to confirm one of the two directions from the first tracer. Tracer results from the third sector do not necessarily have to be used; otherwise, they may be used to verify the result or to achieve a higher accuracy in cases where one of the other tracers is totally leached from the PFM or highly retarded and exhibiting little if any transport. If three tracers are used for the determination of the direction, it is theoret-

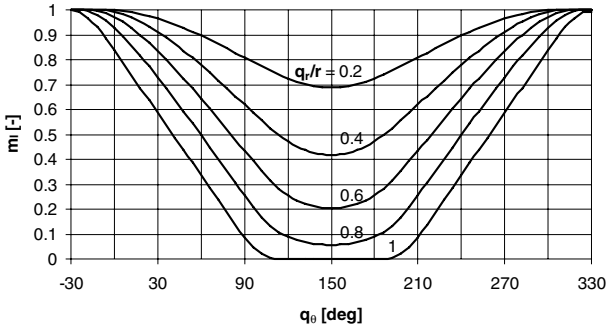

Fig. 25. m_I as a function of q_θ for certain q_r/r's.

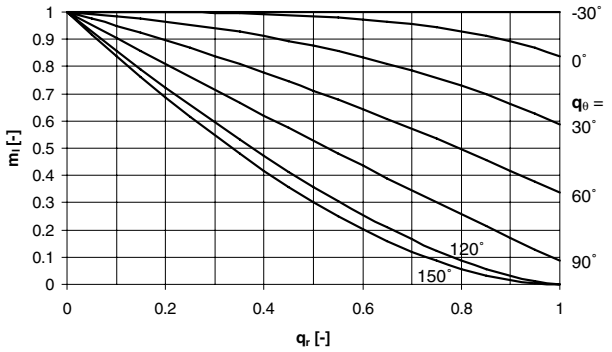

Fig. 26. m_{I} as a function of q_{r}/r for certain q_{θ}'s.

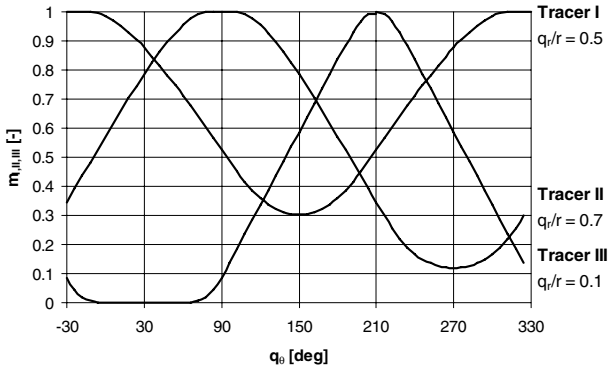

Fig. 27. m_{I}, m_{II} and m_{III} for different retardations of the tracers in the sectors.

ically not necessary to use a fourth tracer over the entire cross-section for the flux (q_{r}) determination. However, it might be advantageous to keep this measurement of flux independent from the measurement of the direction, especially if tracers with different retardations are used. Therefore, it is probably more economical to use three tracers: one over the entire cross-section to measure the flux and the other two in their respective sectors. Thus, the measurement of the flux is kept independent from the measurement of the direction and, in addition, the "m" of the third sector may be evaluated knowing how much of each of the three tracers has been leached out and using their respective retardations. Furthermore, the tracers used for estimating the direction of the flow should have retardation factors, which are similar enough to avoid situations where one tracer is completely eluted from the PFM while another tracer has practically not been eluted at all. This condition provides similar q_{r}'s for the tracers, which translates into similar amplitudes of the elution characteristics in Fig. 27 for the tracers in the individual sectors.

4. Discussion of results and summary

Comparison of Figs. 12–14 for the ring configuration and Figs. 25–27 for the sector configuration shows that both alternatives are practically equivalent as to their theoretical potential to estimate the direction of flow. A minor exception to that may be the fact that with the ring configuration only two of the three measured tracer masses can be used for the directional estimate (since the third tracer mass is always practically zero), while with the sector configuration the third tracer mass can be used to verify the result. From a practical standpoint, the sector configuration presents the advantage that a single tracer extraction is performed for the whole PFM cross section, while for the ring configuration extractions must be done separately for the four sub areas. Furthermore, the sector configuration can be seen to be simpler and, therefore, more convenient in its construction. However, with the sector configuration, additional tracers of similar retardations are required which is not the case with the ring configuration. Neither the sector nor the ring configuration impact the measurements of the magnitudes of groundwater and contaminant mass fluxes as described in the original PFM configuration [9,2].

The fact that in both Figs. 14 and 27 portions of the curves do not exhibit sensitivity to the flow direction (curves horizontal) does not invalidate the ability to estimate the underlying flow direction, since there are always the other two curves which do represent more or less sensitivity to the flow direction. However, independent of ring or sector configuration, this is only true for the range considered here of $q_{\mathrm{r}}/r < 1$; for $q_{\mathrm{r}}/r > 1$ (and the larger q_{r}/r the more likely) situations may occur, where two curves become identical to zero and the even more pronounced ambiguity in the third curve cannot be resolved. For $q_{\mathrm{r}}/r > 2$ all of the tracers are lost from the PFM and no inferences can be made at all, similar to $q_{\mathrm{r}}/r \approx 0$ where not enough tracer displacement has taken place to indicate flow direction. From Figs. 12 and 25 an approximate lower limit of $q_{\mathrm{r}}/r > 0.2$ can be defined to maintain a certain minimum sensitivity of tracer elution with respect to flow direction (this sensitivity increases as q_{r}/r grows, until ambiguities occur at $q_{\mathrm{r}}/r > 1$). This clearly identifies the need to ensure $0.2 < q_{\mathrm{r}}/r < 1$, which can most easily be achieved by inspection of Eq. (37), that is related to Eq. (1) by the "dimensionless cumulative pore volume of fluid intercepted by the device" [9]

$$\frac{q_{\mathrm{r}}}{r} = \frac{\alpha q_0 t_{\mathrm{m}}}{r \Theta R_{\mathrm{d}}} \tag{37}$$

where α [–] is the flow convergence factor according to Hatfield et al. [9] relating the flow rate in the PFM to the ambient flow rate q_0 [L/T] in the aquifer, t_{m} [T] is the duration of the measurement, Θ [–] is the volumetric water content of the PFM, and R_{d} [–] is the retardation coefficient of a given tracer inside the PFM. Eq. (37) expresses the distance q_{r} that a tracer molecule migrates down-gradient using the pore velocity of the water through the PFM ($\alpha q_0/\Theta$) and applying the respective retardation factor R_{d} for a particular tracer. Assuming the hydraulic and geometric properties of the PFM are given, only t_{m} and R_{d} remain to ensure $0.2 < q_{\mathrm{r}}/r < 1$. When q_0 is approximately known (e.g. upper and lower limits) then t_{m} can be chosen for a gi-

ven R_d (or vice versa). If no information about q_0 is available, then different tracers with a range of retardation factors can be applied simultaneously in a PFM in order to provide that enough tracers meet $0.2 < q_r/r < 1$. In both cases it is clear that the respective retardation factors of the applied tracers inside the PFM need to be known for field conditions in order to design and interpret the measurement.

Critical assumptions of the presented theory are that advective transport prevails over diffusive/dispersive transport and that tracer sorption is linear and reaches equilibrium instantaneously. Violation of any of these assumptions undermines the validity of results, since the initial shapes of the tracer plumes (circle and sectors) are not preserved. While the linearity of tracer sorption is simply determined by the respective sorption isotherm, the conditions of purely advective transport and equilibrium sorption are dependent on the magnitude of the water flux through the PFM. For example, dispersion is fractionally proportional to fluid velocity and travel distance and is not expected to be significant for short flows through homogenous PFM sorbents; however, a certain minimum flow rate through the PFM must be provided to safely disregard diffusive contributions to tracer transport, and a certain maximum flow rate must not be exceeded in order to allow for sufficient time to reach sorption equilibrium. The former condition is controlled by the Peclet number P_e [–] and Hatfield et al. [9] specify that in typical field situations ($r = 2.54$ cm; $\Theta = 0.62$; $\alpha = 1$; aqueous phase diffusion coefficient for a resident tracer $D = 1\ \mathrm{cm}^2/\mathrm{d}$) a minimum groundwater flux of approximately 0.7 cm/day is needed to maintain an order of magnitude relative difference between advective and diffusive transport processes (i.e., $P_e = 10$). On the other hand, the latter condition is controlled by the Damkohler number ω [–], which needs to be sufficiently greater than one to ensure a hydraulic residence time of adequate duration to achieve equilibrium tracer sorption/desorption within the PFM; otherwise, water fluxes will be underestimated.

Besides errors due to violations of the underlying assumptions of the theoretical model, errors in the measurement of tracer masses and the PFM orientation in the monitoring well can impact the estimate of groundwater flow direction. Errors in the orientation of the PFM in the well propagate directly to the final estimate of the groundwater flow direction, i.e., any error in the PFM orientation will occur to the same extent in the estimate of flow direction. However, as found by Ballard [3] for the in situ permeable flow sensor, careful installation of the device using rods with marks indicating the orientation of the device during and after installation can limit errors in horizontal device orientation to $\pm 10°$ for depths up to 50 m. On the other hand, errors due to violations of the underlying assumptions will manifest as tracer masses not expected by the model and, such as errors in the tracer mass quantification itself, will propagate through the respective curves for tracer elution of Figs. 14 and 27. Assuming an error-free q_r/r estimate and a certain error in a detected tracer mass, these figures provide a simple graphical means for finding the corresponding error in the flow direction estimate for that tracer. It is easily observed that at first order the resulting error in flow direction is proportional to the respective error in tracer mass and the inverse slope of the corresponding curve at the location in question. In the same way, possible confidence intervals resulting from the analytical tracer mass quantification can be propagated to obtain respective confidence intervals in the flow direction estimate for a given tracer. Assuming errors in the tracer mass quantification that are zero in the mean and comprised in certain intervals, the propagated intervals in the directional estimates from the tracers may be somewhat shifted, but will still overlap around the true flow direction.

In contrast, errors in the compliance of the underlying assumptions of the tracer transport model can cause the estimates of flow direction from the different tracer masses to be inconsistent (or even non-existent in extreme cases). In other words, in situations where the initial shapes of the tracer plumes are not preserved throughout the measurement, the model can lose its ability to explain the actual tracer masses detected in terms of one particular flow direction. This can result in non-overlapping intervals for the directional estimates from the individual tracers. For example, effects of diffusion driven tracer transport in the ring configuration would give non-zero (and in the extreme case of diffusive transport only also equal) tracer masses in each ring sector, which cannot be explained by a single flow direction according to Fig. 14. In this case, the lowest detected tracer mass can be interpreted as the diffusive component of tracer transport. A correction of the tracer masses by setting the lowest tracer mass to zero and subtracting the same value from the other two tracer masses can be attempted in order to eliminate effects of diffusion and possibly facilitate the application of Fig. 14 on the resulting tracer masses. A similar approach for the sector configuration is not straightforward, since with certain flow directions all of the tracers can be eluted advectively and a diffusive component cannot be determined. In the same manner, effects of non-linear and/or non-equilibrium sorption will also introduce discrepancies in the flow direction estimates from each detected tracer mass, but a simple way of correction was not found.

A detailed discussion of uncertainties and error propagation in the estimate of the magnitude of groundwater flux (q_r/r) is contained in Hatfield et al. [9]. Its effects for the present purpose of estimating the direction of groundwater flow are best evaluated by inspection of Figs. 12 and 13 for the ring configuration and the analogous Figs. 25 and 26 for the sector configuration. In an analogous way as discussed above, these figures can be used to directly obtain errors in flow direction estimates for given individual tracer masses and known errors in q_r/r. Furthermore, an error in q_r/r is equivalent in its effects to a violation of the model assumptions on tracer transport in the sense that

it leads to inconsistent estimates of flow direction from the three tracer masses. However, in summary, it is observed that confidence intervals in the tracer mass quantification can be propagated into respective confidence intervals in the estimates of flow direction for each tracer mass, while noncompliance with model assumptions propagates into inconsistent (different) estimates of flow direction for the three tracer masses. The combined effect of these errors can be used to evaluate the uncertainty associated with a flow direction measurement. For example, if tracer mass quantification is known to be accurate and if the flow directions indicated by the three tracer masses are consistent, then the resulting estimate of flow direction can be considered more reliable than otherwise. In fact, it is suggested that the maximum spread in directional estimates given from the two most sensitive tracers be used to quantify an approximate confidence interval for the flow direction estimate (remember that the sensitivity of the third tracer is usually close to zero). In extreme situations, where no consistency is left in the directional estimates from the individual tracers, the method indicates its own inability to give an accurate estimate of flow direction, which can potentially avoid severe misinterpretations. It is believed that under optimal conditions, the accuracy of flow direction measurements using either ring or sector configuration will be of approximately $\pm 15°$.

The center of mass approximation by Campbell et al. [5] is seen to be an acceptable method for the estimation of the flow direction from the PFM data in terms of tracer masses. Fig. 15 shows that, when compared to the geometrically exact result, the systematic error of the approximation vanishes in the directions that coincide with the directions of any axis of symmetry of the PFM cross section. For other cases the maximum error lies within a range of circa $\pm 20°$. The advantages of the center of mass method are that it does not require preliminary determination of the average flow rate to evaluate q_r, and that it does not necessarily rely on the assumption that the circular shape of the tracer plume is preserved. This fact may gain importance when the initial assumptions of linear, instantaneous and reversible tracer sorption and pure convective transport are no longer valid.

While Eq. (1) relates the remaining tracer mass in a PFM (or the center circle of the PFM for the ring configuration) to the volume of water conveyed through the PFM, i.e. the cumulative water flux through the PFM, the actual magnitude of interest in field studies is the ambient groundwater flux in the aquifer. In general, an observation well with a PFM installed represents a disturbance of the ambient groundwater flow field with a certain flow convergence towards or flow divergence around the well. Hence, depending on the geometric and hydraulic properties of the observation well and the PFM with respect to the aquifer, the measured flow rate inside a PFM will be higher or lower than in the undisturbed aquifer. To account for this discrepancy Drost et al. [6] give expressions for flow convergence factors for open observation wells of different configurations, which are adopted by Hatfield et al. [9] to include the presence of a PFM in the well. While the magnitude of flow convergence or divergence affects the measurement of flow direction through the estimate of q_r/r, the qualitative properties (i.e., the shape) of the flow field inside the PFM also have an impact on the tracer elution process. As further pointed out by Hatfield et al. [9], potential theoretical considerations (e.g. [14]) show, that the flow field inside the PFM cross section is uniform, independent of the permeability contrast to the aquifer. This allows for the application of the rectilinear stream tube tracer transport model in Hatfield et al. [9] and the present study. A possible scenario, where the measured flow direction inside the PFM may be different to the ambient groundwater flow direction in the aquifer, can occur in aquifers with horizontally anisotropic hydraulic conductivities and when neither of the principal axes of anisotropy is aligned with the direction of the hydraulic gradient. In such cases the direction of ambient groundwater flow deviates from the direction of the hydraulic gradient and the measured flow direction in the (isotropic) PFM rather indicates the direction of the hydraulic gradient than that of the ambient groundwater flow.

Two fundamental assumptions for the measurement of both magnitude and direction of groundwater flow using the PFM method are that variations in the flow direction during the measurement period are small and that the vertical component of flow inside the PFM can be neglected with respect to the horizontal component. The former assumption is likely to be violated with long term (e.g. seasonal) monitoring, while it is also crucial for the present purpose of measuring one particular flow direction. As a consequence, if the primary purpose of the measurement is to determine the groundwater flow direction, it may be favorable to design the PFM for shorter monitoring periods. The latter assumption is easily violated by fluctuations of the water table or when different hydraulic horizons separated by aquitards are penetrated by a monitoring well. Deploying impermeable packers at certain intervals along the PFM axis can mitigate the effect of vertical flow inside the PFM. However, both variations in flow direction as well as vertical flow inside the PFM are factors that undermine the validity of measurements and both need to be taken into account under field conditions [9].

Further work will need to conduct laboratory and field tests with both configurations to validate the practical usefulness of the proposed methods and to collect practical experience in connection with the construction of the PFMs and their installation techniques in the field.

Acknowledgements

This research was partially the by the US Department of Defense (Project No. ER0114) under the Environmental Security Technology Compliance Program (ESTCP) and the Florida Water Resources Research Center under a Grant from the US Department of Interior (01HqGR0138).

References

[1] Alden AS, Munster CL. Field test of the in-situ permeable ground water flow sensor. Ground Water Monitor Remed 1997;17(4):81–8.

[2] Annable MD, Hatfield K, Cho J, Klammler H, Parker BL, Cherry JA, et al. Field-scale evaluation of the passive PFM for simultaneous measurement of groundwater and contaminant fluxes. Environ Sci Technol 2005;39(18):7194–201.

[3] Ballard S. The in-situ permeable flow sensor: a groundwater flow velocity meter. Ground Water 1996;34(2):231–40.

[4] Basu N, Rao PSC, Poyer IC, Annable MD, Hatfield K. Flux-based assessment at a manufacturing site contaminated with trichloroethylene. J Contam Hydrol 2006;86(1–2):105–27.

[5] Campbell T, Hatfield K, Klammler H, Annable MD, Rao PSC. Magnitude and directional measures of water and Cr(VI) fluxes by passive PFM. Environ Sci Technol [in press]. doi:10.1021/es0602686.

[6] Drost W, Klotz D, Koch A, Moser H, Neumaier F, Rauert W. Point dilution methods of investigating ground water flow by means of radioisotopes. Water Resour Res 1968;4:125–46.

[7] Davis GB, Barber C, Power TR, Thierrin J, Patterson BM, Rayner JL, et al. The variability and intrinsic remediation of a BTEX plume in anaerobic sulphate-rich groundwater. J Contam Hydrol 1999;36(3–4):265–90.

[8] Guthry M. Use of a geo flowmeter for the determination of ground water flow direction. Ground Water Monitor Rev 1986;6(2):81–6.

[9] Hatfield K, Annable M, Cho J, Rao PSC, Klammler H. A direct passive method for measuring water and contaminant fluxes in porous media. J Contam Hydrol 2004;75:155–81.

[10] Kerfoot WB. Comparison of 2-D and 3-D ground water flow meter probes in fully penetrating monitoring wells. Proceedings of the second national symposium an aquifer restoration and ground water monitoring. Worthington (OH): Water Well Journal Publishing Co.; 1982. p. 264–8.

[11] Kerfoot WB. Monitoring well construction, and recommended procedures for direct ground water flow measurements using a heat-pulsing flow meter. Ground water contamination field methods. ASTM special technical publication, vol. 963. Philadelphia (PA): American Society for Testing and Materials; 1988. p. 146–61.

[12] Lamontagne S, Dighton J, Ullman W. Estimation of groundwater velocity in riparian zones using point dilution tests. CSIRO Land and Water, Technical Report 14/02; 2002.

[13] SonTek, Inc."Modified ADV for 3D velocity measurements in boreholes – Final Project Report". US Geological Survey, Contract Number 1434-95-C-40232; 1996. p. 29.

[14] Strack ODL, Haitjema HM. Modeling double aquifer flow using a comprehensive potential and distribution singularities: 2. Solution for inhomogeneous permeabilities. Water Resour Res 1981;17(5):1551–60.

[15] Thierrin J, Davis GB, Barber C. A groundwater tracer test with deuterated compounds for monitoring in-situ biodegradation and retardation of aromatic compounds. Ground Water 1995;33(3):469–75.

[16] US Department of Energy – Oak Ridge National Laboratory. 1993. Technology Information Profile (rev. 2) for ProTech, Technology Name – Colloidal Borescope. DOE ProTech Database, TTP Reference Number OR – 11211 – 04, July 15.

[17] US Department of the Interior. 1999. An evaluation of borehole flowmeters used to measure horizontal groundwater flow in limestone of Indiana, Kentucky, and Tennesee. Water Resources Investigators Report 01-4139.

[18] White PA. Electrode arrays for measuring ground water flow direction and velocity. Geophysics 1994;59(2):192–201.